

A method to determine wall shear stress from mean profiles in turbulent boundary layers

Praveen Kumar · Krishnan Mahesh

Received: date / Accepted: date

Abstract The direct measurement of wall shear stress in turbulent boundary layers (TBL) is challenging, therefore requiring it to be indirectly determined from mean profile measurements. Most popular methods assume the mean streamwise velocity to satisfy either a logarithmic law in the inner layer or a composite velocity profile with many tuned constants for the entire TBL, both of which require reliable data from the inner layer. The presence of roughness and pressure gradient brings additional complications where most existing methods either fail or require significant modification. A novel method is proposed to determine the wall shear stress in zero pressure gradient TBL from measured mean profiles, without requiring near-wall data. The method is based on the stress model of Kumar and Mahesh [Phys. Rev. Fluids 6, 024603 (2021)], who developed accurate models for mean stress and wall-normal velocity in zero pressure gradient TBL. The proposed method requires a single point measurement of mean streamwise velocity and mean shear stress in the outer layer, preferably between 20 to 50% of the TBL, and an estimate of boundary layer thickness and shape factor. The method can handle wall roughness without modification and is shown to predict friction velocities to within 3% over a range of Reynolds number for both smooth and rough wall zero pressure gradient TBL. In order to include the pressure gradient effects, the work of Kumar and Mahesh [Phys. Rev. Fluids 6, 024603 (2021)] is revisited to derive a novel model for both mean stress and wall-normal velocity in pressure gradient TBL, which is then used to formulate a method to obtain the wall

shear stress from the profile data. Overall, the proposed method is shown to be robust and accurate for a variety of pressure gradient TBL.

Keywords Turbulent boundary layer · Wall shear stress

1 Introduction

Flow over a solid surface or wall produces a thin region of high shear close to the wall due to no-slip conditions imposed at surface by viscosity. This thin near-wall ‘boundary layer’ has been extensively studied since the seminal work of Prandtl (Prandtl, 1904). The high shear induces large tangential stresses at the wall, which leads to drag and energy expenditure in aerodynamic and hydrodynamic applications. Under most practical conditions, the boundary layer is turbulent, and is commonly described using first- and second-order flow field statistics (Pope, 2001).

In turbulent boundary layers, the skin-friction is represented by the friction velocity defined as $u_\tau = \sqrt{\tau_w/\rho}$ where τ_w is the mean wall-stress and ρ is density of the fluid. u_τ is a very important velocity scale in TBL due to its common use in most scaling laws. Unfortunately, the direct measurement of u_τ is often not feasible, requiring indirect methods to determine it. Although a number of indirect techniques are available for determining u_τ , none are universally accepted.

An indirect technique can be formulated if the behavior of the mean velocity profile is known in viscous units. Several so called ‘law of the wall’ have been proposed for the inner layer (typically $y/\delta < 0.15$) that relate the inner scaled mean streamwise velocity (U^+) to wall normal coordinate (y^+), where ‘+’ denotes normalization with u_τ and ν . Table 1 list some of the pop-

Praveen Kumar · Krishnan Mahesh
Department of Aerospace Engineering and Mechanics,
University of Minnesota, Minneapolis, Minnesota 55455, USA
E-mail: kmahesh@umn.edu

ular formulae for the law of the wall. The readers are referred to Zhang et al. (2021) for a more extensive list.

Boundary layer researchers commonly use the Clauser chart method (Fernholz and Finley, 1996), which assumes that the mean velocity satisfies the universal logarithmic law

$$U^+ = \frac{1}{\kappa} \ln y^+ + B \quad (1)$$

over the range $y^+ > 30$ and $y/\delta \leq 0.15$, where $\kappa \approx 0.4$ and $B \approx 5$. The exact values of the constants κ and B , their universality, and the exact region of validity of Eq. (1) have been widely debated in the literature (Smits et al., 2011). Table 2 shows some of the popular values of the constants for zero pressure gradient TBL and region of validity. Using the Clauser chart method, u_τ is determined to be the value that best fits the measured mean streamwise velocity profile to Eq. (1) in its range of validity. For example, De Graaff and Eaton (2000) obtained u_τ using the Clauser chart method by fitting the mean velocity data to Eq. (1) in the region $y^+ > 50$ and $y/\delta < 0.2$ with $\kappa = 0.41$ and $B = 5$.

Several researchers have recognized and documented the limitations of the Clauser chart method. George and Castillo (1997) showed clear discrepancies between mean velocity profiles scaled using direct measurements of u_τ and approximations using the Clauser chart method. Wei et al. (2005) explicitly illustrated how the Clauser chart method can mask subtle Re -number-dependent behavior, causing significant error in determining u_τ . Several past works have attempted to improve the Clauser chart method by optimizing the constants of Eq. 1. Rodríguez-López et al. (2015) analyzed several such past efforts and proposed a better method by optimizing the various parameters appearing in the mean velocity profile of the entire TBL. However, as mentioned by the authors themselves, their method was sensitive to the assumed universal velocity profile, and the definition of the error which was used for the optimization.

A more recent approach to determine u_τ (e.g. Samie et al. 2018) is to fit the entire mean streamwise velocity profile to the composite profile of Chauhan et al. (2009):

$$U_{composite}^+ = U_{inner}^+ + \frac{2II}{\kappa} W(\eta), \quad (2)$$

where,

$$U_{inner}^+ = \frac{1}{\kappa} \ln \left(\frac{y^+ - a}{-a} \right) + \frac{R^2}{a(4\alpha - a)} \left[(4\alpha + a) \ln \left(-\frac{a}{R} \frac{\sqrt{(y^+ - \alpha)^2 + \beta^2}}{y^+ - a} \right) + \frac{\alpha}{\beta} (4\alpha + 5a) \left(\arctan \left(\frac{y^+ - \alpha}{\beta} \right) + \arctan \left(\frac{\alpha}{\beta} \right) \right) \right], \quad (3)$$

with $\alpha = (-1/\kappa - a)/2$, $\beta = \sqrt{-2a\alpha - \alpha^2}$, and $R = \sqrt{\alpha^2 + \beta^2}$. The chosen values of $\kappa = 0.384$ and $a = -10.3061$. The wake function W is given by

$$W(\eta) = \left[\left(1 - \exp(-(1/4)(5a_2 + 6a_3 + 7a_4)\eta^4 + a_2\eta^5 + a_3\eta^6 + a_4\eta^7) \right) / \left(1 - \exp(-(a_2 + 2a_3 + 3a_4)/4) \right) \right] \left(1 - \frac{1}{2II} \ln \eta \right), \quad (4)$$

where $a_2 = 132.8410$, $a_3 = -166.2041$, $a_4 = 71.9114$, the wake parameter $II = 0.45$ and $\eta = y/\delta$. Chauhan et al. (2009) have also shown that the accuracy of the approach to be within $\pm 2\%$ of those determined by direct measurements. Although the method appears attractive, it still requires accurate near-wall measurements to determine u_τ reliably. Moreover, the method can not be used for rough wall and pressure gradient TBL.

Several recent studies (e.g. Fukagata et al., 2002; Mehdi and White, 2011; Mehdi et al., 2014) have attempted to relate u_τ to measurable profile quantities using the governing equations of the mean flow. These methods often require additional measurements and assumptions to account for the unknown quantities. For example, Mehdi and White (2011) and Mehdi et al. (2014) obtained u_τ using the measured mean streamwise velocity and Reynolds shear stress profiles. However, their method was sensitive to noisy or missing near-wall data. They overcome this limitation by assuming a shape for the total shear stress profile and by smoothing the measured data.

The presence of pressure gradient makes the indirect determination of u_τ from profile measurements more challenging. Clauser chart method requires significant modifications before it can be employed for obtaining u_τ for any pressure gradient TBL. Several non-dimensional parameters have been proposed in literature to quantify pressure gradient effects on TBL. These parameters only differ in length and velocity scales used to normalize the freestream pressure gradient (dP_e/dx). Some of the popular pressure gradient parameters are

$$\beta = \frac{\delta^*}{\rho u_\tau^2} \frac{dP_e}{dx}, \quad (5)$$

$$K = -\frac{\nu}{\rho U_e^3} \frac{dP_e}{dx}, \quad (6)$$

$$p_x^+ = \frac{\nu}{\rho u_\tau^3} \frac{dP_e}{dx}. \quad (7)$$

Here, ρ is the fluid density, δ^* is the displacement thickness, ν is the kinematic viscosity, U is the streamwise velocity and the subscript ‘e’ denotes the value at the edge of the boundary layer (δ), which is defined as the

Table 1 Popular formulae for the law of the wall.

Authors	Formulae	Region where valid
Prandtl (1910)	$U^+ = y^+$	$0 \leq y^+ \leq 11.5$
Taylor (1916)	$U^+ = 2.5 \ln y^+ + 5.5$	$y^+ \geq 11.5$
von Kármán (1939)	$U^+ = y^+$	$0 \leq y^+ < 5$
	$U^+ = 5 \ln y^+ - 3.05$	$5 \leq y^+ < 30$
	$U^+ = 2.5 \ln y^+ + 5.5$	$y^+ \geq 30$
Rannie (1956)	$U^+ = 1.454 \tanh(0.0688 y^+)$	$0 \leq y^+ < 27.5$
	$U^+ = 2.5 \ln y^+ + 5.5$	$y^+ \geq 27.5$
Werner and Wengle (1993)	$U^+ = y^+$	$0 \leq y^+ < 11.81$
	$U^+ = 8.3(y^+)^{1/7}$	$y^+ \geq 11.81$
Reichardt (1951)	$U^+ = 2.5 \ln(1 + 0.4 y^+) + 7.8(1 - e^{-y^+/11} - (y^+/11)e^{-0.33 y^+})$	$y^+ \geq 0$
Spalding (1961)	$y^+ = U^+ + 0.1108 \left(e^{0.4 \kappa U^+} - 1 - \kappa U^+ - \frac{(\kappa U^+)^2}{2} - \frac{(\kappa U^+)^3}{6} - \frac{(\kappa U^+)^4}{24} \right)$	$y^+ \geq 0$
Monkewitz et al. (2007)	$U_{inner}^+ = U_{inner,23}^+ + U_{inner,25}^+$, where $U_{inner,23}^+ = 0.68285472 \ln(y^{+2} + 4.7673096 y^+ + 9545.9963)$ $+ 1.2408249 \arctan(0.010238083 y^+ + 0.024404056)$ $+ 1.2384572 \ln(y^+ + 95.232690) - 11.930683$ $U_{inner,25}^+ = -0.50435126 \ln(y^{+2} - 7.8796955 y^+ + 78.389178)$ $+ 4.7413546 \arctan(0.12612158 y^+ - 0.49689982)$ $- 2.7768771 \ln(y^{+2} + 16.209175 y^+ + 933.16587)$ $+ 0.37625729 \arctan(0.033952353 y^+ + 0.27516982)$ $+ 6.5624567 \ln(y^+ + 13.670520) + 6.1128254$	$y^+ \geq 0$

Table 2 Values of the log law constants in TBL.

Authors	Formulae	Region where valid
Coles (1956)	$\kappa = 0.41, B = 5$	$50 < y^+ < 0.2 Re_\tau$
Österlund (1999)	$\kappa = 0.38, B = 4.1$	$50 \leq y^+ \leq 0.15 Re_\tau$
Nagib et al. (2007)	$\kappa = 0.384, B = 4.173$	$50 \leq y^+ \leq 0.15 Re_\tau$
Marusic et al. (2013)	$\kappa = 0.39, B = 4.3$	$3 Re_\tau^{1/2} < y^+ < 0.15 Re_\tau$
Monkewitz et al. (2007)	$\kappa = 0.384, B = 4.17$	$50 \leq y^+ \leq 0.15 Re_\tau$
Monkewitz (2017)	$\kappa = 0.384, B = 4.22$	$50 \leq y^+ \leq 0.15 Re_\tau$

wall-normal location where $U = 0.99U_e$. In the present work, the Rotta–Clauser pressure gradient parameter (β) (Rotta, 1953; Clauser, 1954) is used, which is common in literature for near-equilibrium TBL. It is important to understand that one requires knowledge of u_τ to obtain β , which is not available *a priori*. Therefore, experimental studies often use the acceleration parameter K to quantify pressure gradient. It can be readily seen that they are related as

$$\beta = -K Re_{\delta^*} \frac{U_e^2}{u_\tau^2}, \quad (8)$$

where, Re_{δ^*} is the displacement thickness based Re .

Volino and Schultz (2018) used integral analysis of the mean streamwise momentum equation to obtain a relation between mean velocity and Reynolds shear stress profiles, that was subsequently used to determine u_τ from measured profiles. The utility of the method was shown through application to experimental data including zero pressure gradient cases from smooth and rough walls, and smooth wall cases with favorable and adverse pressure gradients. Although their method is generally applicable, it has two main issues: (i) the for-

mulation attempts to minimize dependence on streamwise gradients, but some dependence remains, making data from two or more streamwise locations necessary and the process of determining u_τ iterative, and (ii) since the method requires numerical integration of the profiles in the wall-normal direction, the accuracy deteriorates if near-wall data is omitted. In order to improve the accuracy in such cases, they either used the trapezoidal rule or an assumed velocity profile to account for the missing contribution. The requirement to have data at multiple streamwise locations to obtain streamwise gradients was mitigated by Womack et al. (2019) by essentially using a skin-friction law and connecting the streamwise gradient to the wall-normal gradient using a universal W . However, this makes the method sensitive to the choice of W and the constants in the law of the wall.

It is clear that most of the issues in determining u_τ from profile data stem from the presumption of a universal mean velocity profile that is valid in the inner layer or throughout the TBL. Therefore, a method is proposed to determine u_τ from mean profile measurements without any assumption of a universal mean

velocity profile, thereby avoiding all issues associated with uncertainties in the constants of the assumed profile. The method utilizes profiles of the mean velocity and the mean shear stress without requiring any near-wall ($\eta < 0.2$) data, which is challenging to acquire at high Re (Vallikivi et al., 2015; Samie et al., 2018). Presence of wall roughness and pressure gradients brings additional complications. The method is based on integral analysis of the streamwise momentum equation but does not require profiles at multiple streamwise locations, wall-normal integration of data or any iterative procedure to determine u_τ accurately. The method is also shown to be general enough to include wall roughness and is extended to include pressure gradient gradients.

The paper is organized as follows. The proposed method for zero pressure gradient (ZPG) TBL is described in Section 2. Section 3 describes the databases used in the present work. The performance of the proposed method for smooth and rough wall ZPG TBL is discussed in Section 4. In order to extend the method for pressure gradient TBL, a novel model each for mean stress and wall-normal velocity is first derived, which is subsequently used to propose a method to determine u_τ and assess its performance in a variety of pressure gradient TBL cases in Section 5. Section 6 concludes the paper.

2 The proposed method for ZPG TBL

The boundary layer approximations for the time-averaged Navier–Stokes equations in Cartesian coordinates yield

$$\frac{\partial U}{\partial x} + \frac{\partial V}{\partial y} = 0, \quad (9)$$

$$U \frac{\partial U}{\partial x} + V \frac{\partial U}{\partial y} = -\frac{1}{\rho} \frac{dP}{dx} + \frac{\partial T}{\partial y}, \quad (10)$$

where U and V are the streamwise (x) and the wall-normal (y) components of mean velocity vector, ρ is the fluid density, P is the mean pressure and T is the mean total stress, i.e., the sum of the viscous stress ($\nu \partial U / \partial y$) and the Reynolds shear stress ($-\overline{u'v'}$). Using Eqs. (9) and (10), and neglecting the terms containing pressure gradient and wall-normal velocity, it can be shown that

$$\frac{\partial T}{\partial y} = -U_e \frac{\partial V}{\partial y} + (U_e - U) \frac{\partial V}{\partial y}. \quad (11)$$

(δ), which is defined as the wall-normal location where $U = 0.99U_e$. Integrating Eq. (11) from a generic y to $y = \delta$ and normalizing in viscous units yield

$$T^+ = U_e^+ V_e^+ \left(1 - \frac{V}{V_e}\right) - \int_{y^+}^{\delta^+} (U_e^+ - U^+) \frac{\partial V^+}{\partial y^+} dy^+ \quad (12)$$

where the second term requires modeling. Kumar and Mahesh (2021) used available TBL data to model the second term in the rhs of Eq. (12) to obtain a modeled total stress,

$$T^+ = H(1 - V/V_e) + (H - 1)(\eta - 1) \quad (13)$$

where, $\eta = y/\delta$ and H is the shape factor defined as the ratio of δ^* and momentum thickness (θ). Note that the relation $U_e^+ V_e^+ = H$ (Wei and Klewicki, 2016; Kumar and Mahesh, 2018) is used in Eq. (13). The mean shear stress model was validated for a range of Re using past simulations and experiments. Since, most past work do not report the V profile, Kumar and Mahesh (2021) also provided a compact model for V/V_e as function of y/δ , i.e.,

$$\frac{V}{V_e} = \tanh(a\eta + b\eta^3), \quad (14)$$

where the model constants $a = 0.5055$ and $b = 1.156$. Now, Eq. (13) can be rearranged to obtain

$$u_\tau = \sqrt{\frac{T}{H(1 - V/V_e) + (H - 1)(\eta - 1)}}. \quad (15)$$

Figure 1 shows the rhs of Eq. (15) for cases S1000, S2000, S3030 and S4060 (i.e. $Re_\theta = 1006$ to 4061, (see Table 3) using actual V/V_e (Figure 1 (a)) and modeled V/V_e (Figure 1 (b)) using Eq. (14). The true values of u_τ are also shown for comparison. Each symbol represents u_τ predicted using data point at only that location in the boundary layer. It is clear that Eq. (15) predicts $u_{\tau au}$ accurately for any data point in the range $y/\delta < 0.6$. It is also evident that as Re increases, the difference between the u_τ obtained using actual V/V_e and modeled V/V_e becomes increasingly smaller. Since V is often not available, all subsequent results in this paper use modeled V (Eq. (14)).

The proposed method determines u_τ from Eq. (15). In principle, only one measurement location anywhere in the range $y/\delta < 0.6$ is sufficient to obtain u_τ as observed in figure 1. However, if a coarse profile measurement is available, u_τ value is the horizontal line which best fits the rhs of Eq. (15) data in the range $0.2 < y/\delta < 0.5$. The region $y/\delta < 0.2$ is deliberately avoided since data in this region is difficult to acquire in experiments at high Re (Vallikivi et al., 2015; Samie et al., 2018).

3 TBL databases

Table 3 lists the relevant details of all the ZPG direct numerical simulation (DNS) and experimental databases used in this paper. For any TBL, momentum-based

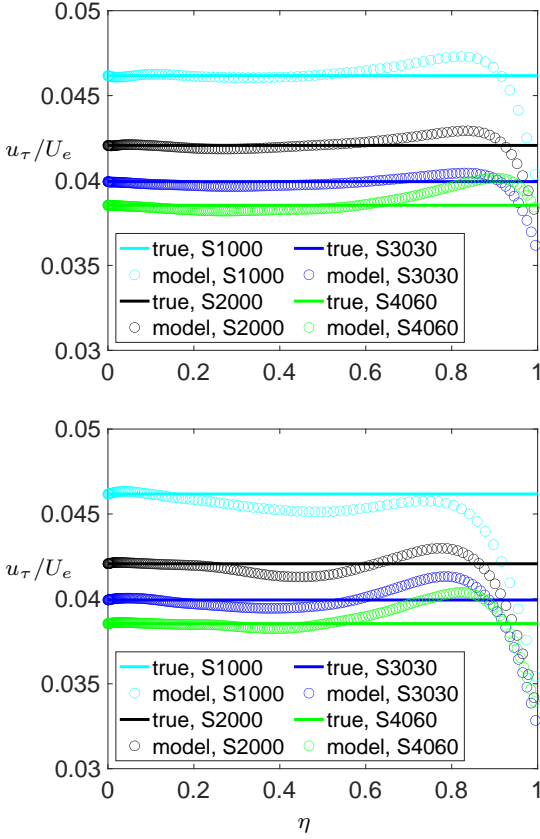


Fig. 1 Profiles of rhs of Eq. (15) (symbols) are compared to true u_τ (lines) for cases S1000, S2000, S3030 and S4060, using actual V/V_e (a) and modeled V/V_e (b) using Eq. (14).

Reynolds number Re_θ and friction-based Reynolds number (Re_τ) are defined as $Re_\theta = U_e \theta / \nu$, and $Re_\tau = u_\tau \delta / \nu$. Note that the correlation $Re_\tau = 1.13 \times Re_\theta^{0.843}$ proposed by Schlatter and Örlü (2010) is used to obtain Re_θ from the reported values of Re_τ in the experiments of Morrill-Winter et al. (2015) and Baidya et al. (2017). All these smooth wall cases are named starting ‘S’ or ‘E’ to represent simulations or experiments respectively, followed by the rounded-off value of Re_θ . The last three cases listed in the table are taken from Flack et al. (2020) who performed experiments on rough wall TBL by systematically changing the surface skewness of a rough surface with same root-mean-square roughness height. These rough wall cases are named started ‘R’ to represent rough, followed by ‘0’, ‘-’ or ‘+’ for zero, negative and positive surface skewness respectively.

Table 4 lists the relevant details of all the APG TBL profiles used in this paper taken from the large eddy simulation (LES) databases of Bobke et al. (2017). Note that Bobke et al. (2017) discussed the effects of the sub-grid stress (SGS) on the dissipation of turbulent ki-

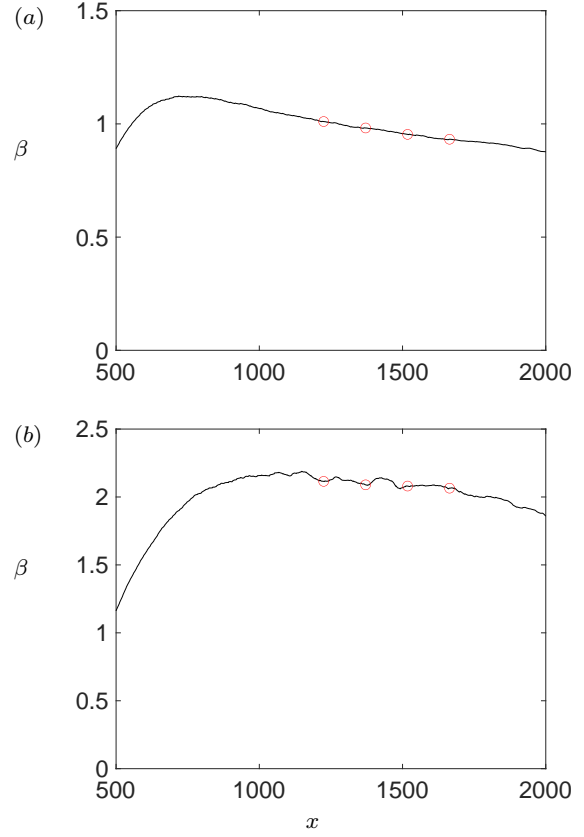


Fig. 2 The streamwise evolution of β is shown for $\beta \approx 1$ and 2 (b) data. The streamwise stations are highlighted with \circ where profiles listed in table 4 are taken from.

netic energy (TKE), concluding that the mesh resolution and the SGS model used in their LES were adequately reproducing the energy transfer across scales. Also, Bobke et al. (2017) had a large region of controlled β making their data suitable for validation.

There are four different flat plate TBL databases listed in Table 4, with four profiles chosen from each case. The case name “ βxy ” denotes y^{th} profile from the database where $\beta \approx x$. Similarly, the case name “ mxy ” denotes y^{th} profile from the database where the freestream follows a power-law $U_e \sim (x - x_0)^m$ with xx indicating the percentage negative value of the exponent m , i.e., profiles with names starting with “m13” are taken from the database where $m = -0.13$ and so on. Re_τ , β and H are listed for all the profiles. Figures 2 and 3 show the streamwise evolution of β for the constant- β and constant- m databases respectively, highlighting the stations where the profiles listed in Table 4 are taken from. The readers are referred to the papers cited in the table for numerical and experimental details. Note that throughout the paper, ‘true u_τ ’ is the value reported in the reference paper.

Table 3 ZPG TBL datasets considered in this paper.

Case	Re_θ	Re_τ	H	Database
S1000	1006	359	1.4499	DNS (Schlatter and Örlü, 2010)
S2000	2001	671	1.4135	DNS (Schlatter and Örlü, 2010)
S3030	3032	974	1.3977	DNS (Schlatter and Örlü, 2010)
S4060	4061	1272	1.3870	DNS (Schlatter and Örlü, 2010)
S5000	5000	1571	1.3730	DNS (Sillero et al., 2013)
S6000	6000	1848	1.3669	DNS (Sillero et al., 2013)
S6500	6500	1989	1.3633	DNS (Sillero et al., 2013)
E6920	6919	1951	1.3741	Expt (Morrill-Winter et al., 2015)
E9830	9826	2622	1.3661	Expt (Morrill-Winter et al., 2015)
E11200	11200	2928	1.3366	Expt (Morrill-Winter et al., 2015)
E15120	15116	3770	1.3350	Expt (Morrill-Winter et al., 2015)
E15470	15469	3844	1.3476	Expt (Morrill-Winter et al., 2015)
E24140	24135	5593	1.3264	Expt (Morrill-Winter et al., 2015)
E26650	26647	6080	1.2938	Expt (Morrill-Winter et al., 2015)
E36320	36322	7894	1.2774	Expt (Morrill-Winter et al., 2015)
E21630	21632	5100	1.3	Expt. (Baidya et al., 2017)
E51520	51524	10600	1.28	Expt. (Baidya et al., 2017)
R0	-	1918	-	Expt. (Flack et al., 2020)
R-	-	1600	-	Expt. (Flack et al., 2020)
R+	-	2202	-	Expt. (Flack et al., 2020)

Table 4 APG TBL datasets considered in this paper.

Case	β	Re_τ	H	Database
β_{11}	1.0104	515.5	1.6024	LES (Bobke et al., 2017)
β_{12}	0.9820	558.3	1.5924	LES (Bobke et al., 2017)
β_{13}	0.9537	599.1	1.5827	LES (Bobke et al., 2017)
β_{14}	0.9322	637.9	1.5738	LES (Bobke et al., 2017)
β_{21}	2.1149	502.5	1.7196	LES (Bobke et al., 2017)
β_{22}	2.0894	545.4	1.7114	LES (Bobke et al., 2017)
β_{23}	2.0805	589.9	1.7024	LES (Bobke et al., 2017)
β_{24}	2.0649	640.3	1.6921	LES (Bobke et al., 2017)
m131	1.2041	527.2	1.6379	LES (Bobke et al., 2017)
m132	1.1416	573.1	1.6202	LES (Bobke et al., 2017)
m133	1.0894	612.2	1.6061	LES (Bobke et al., 2017)
m134	1.0389	654.5	1.5925	LES (Bobke et al., 2017)
m161	2.5889	500.7	1.7831	LES (Bobke et al., 2017)
m162	2.4825	547.7	1.7669	LES (Bobke et al., 2017)
m163	2.3660	596.6	1.7459	LES (Bobke et al., 2017)
m164	2.2192	644.8	1.7259	LES (Bobke et al., 2017)

4 Method performance for ZPG TBL

4.1 Smooth wall TBL

Figure 4 shows the predicted u_τ for TBL cases ranging from $Re_\theta = 1006$ to 4061 using the DNS data of Schlatter and Örlü (2010). The black lines show the bounds of $\pm 3\%$ deviation from the true values. Figure 5 shows similar results for TBL cases ranging from $Re_\theta = 5000$ to 6500 using the DNS data of Sillero et al. (2013). In all these cases, the proposed method accurately predicts u_τ using the DNS data in the range $0.2 < \eta < 0.6$.

Next, the proposed method is used to predict u_τ using the experimental database of Morrill-Winter et al.

(2015) and Baidya et al. (2017). Note that both these experimental campaigns used the composite fit method to determine u_τ . Figures 6 and 7 show the predicted u_τ compared for the experimental data of Morrill-Winter et al. (2015). Overall, the proposed method agrees to the data obtained from the composite fit approach to within 3% in the region $0.2 < \eta < 0.5$ for all the cases except E36320, where it is within 3% in the region $0.2 < \eta < 0.35$.

Figure 8 shows the predicted u_τ compared to the experimental data of Baidya et al. (2017). Note that the contribution of viscous stress to the total stress is ignored for these data sets. Overall, the proposed method agrees with the composite fit approach to within 3% in the region $0.2 < \eta < 0.35$.

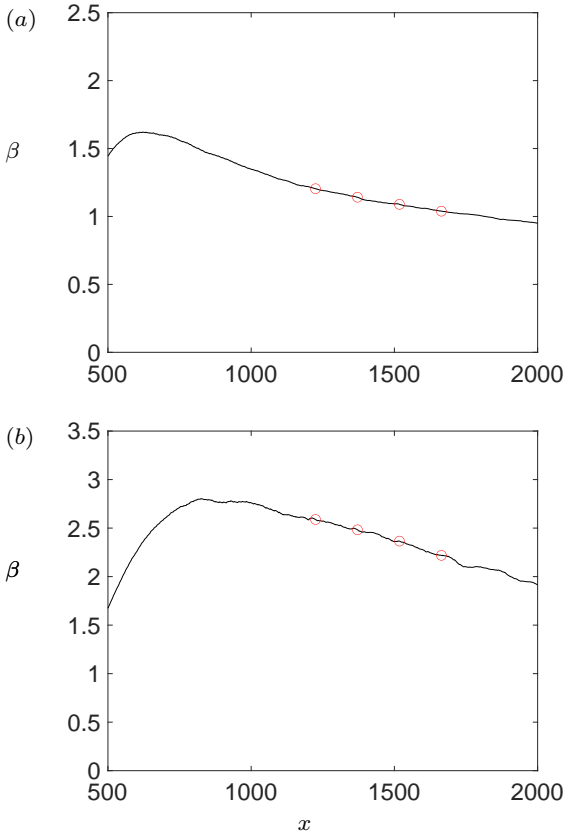


Fig. 3 The streamwise evolution of β is shown for $m \approx -0.13$ and -0.16 data. The streamwise stations are highlighted with \circ where profiles listed in table 4 are taken from.

4.2 Rough wall TBL

Flack et al. (2020) performed experiments on rough wall TBL where u_τ values were determined using the modified Clauser chart method of Perry and Li (1990) as described in Schultz and Flack (2003) in detail. The method uses the velocity profile in the log-law region in an iterative procedure to obtain both u_τ and the wall offset i.e. the location in the roughness where $y = 0$. The reported uncertainty in u_τ for the modified Clauser chart method was $\pm 4\%$.

Figure 9 shows the performance of the proposed method for rough wall TBL data of Flack et al. (2020). Note that the contribution of viscous stress in T is neglected. As observed in Figure 9, the proposed method shows good performance in the range $0.2 < \eta < 0.5$ for all the rough wall TBL cases. Since the original paper does not report H , $H = 1.38$ is used for all these cases. This value is chosen as it is close to smooth wall case at similar Re_τ listed in Table 3. It will be shown later in section 4.3 that the proposed method is relatively insensitive to H . It is remarkable

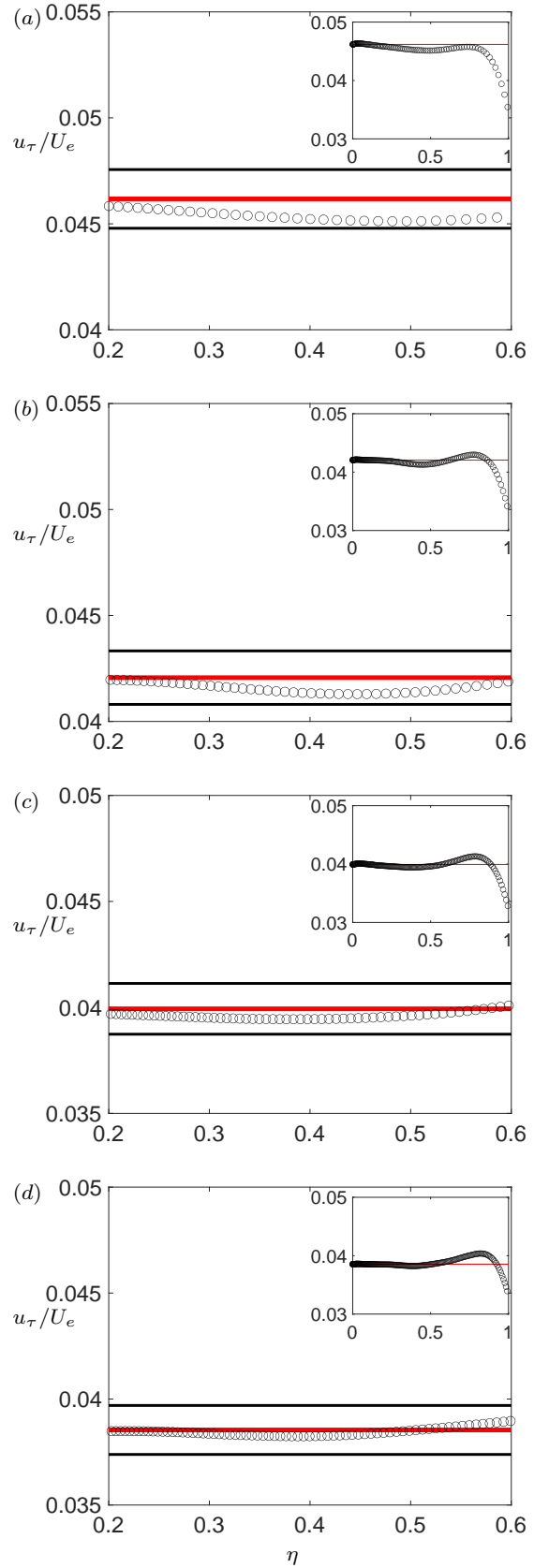


Fig. 4 Predicted u_τ is compared to true u_τ (red line) for cases S1000 (a), S2000 (b), S3030 (c), and S4060 (d). Note that the black lines show $\pm 3\%$ of the red line.

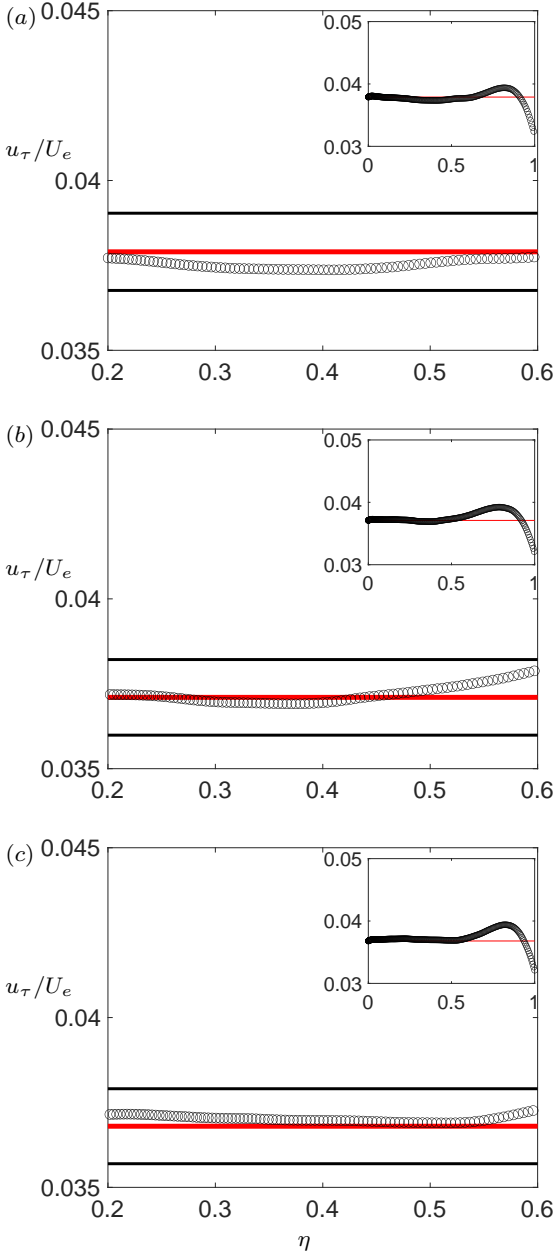


Fig. 5 Predicted u_τ is compared to true u_τ (line) for cases S5000 (a), S6000 (b), and S6500 (c). Note that the black lines show $\pm 3\%$ of the red line.

that the method is able to handle wall roughness accurately without requiring any modification.

4.3 Sensitivity to TBL parameters

An important point to note is that the proposed method requires the knowledge of H in addition to δ . From the definition of δ^* and θ , it is clear that the near-wall region contributes more to the former. Obtaining

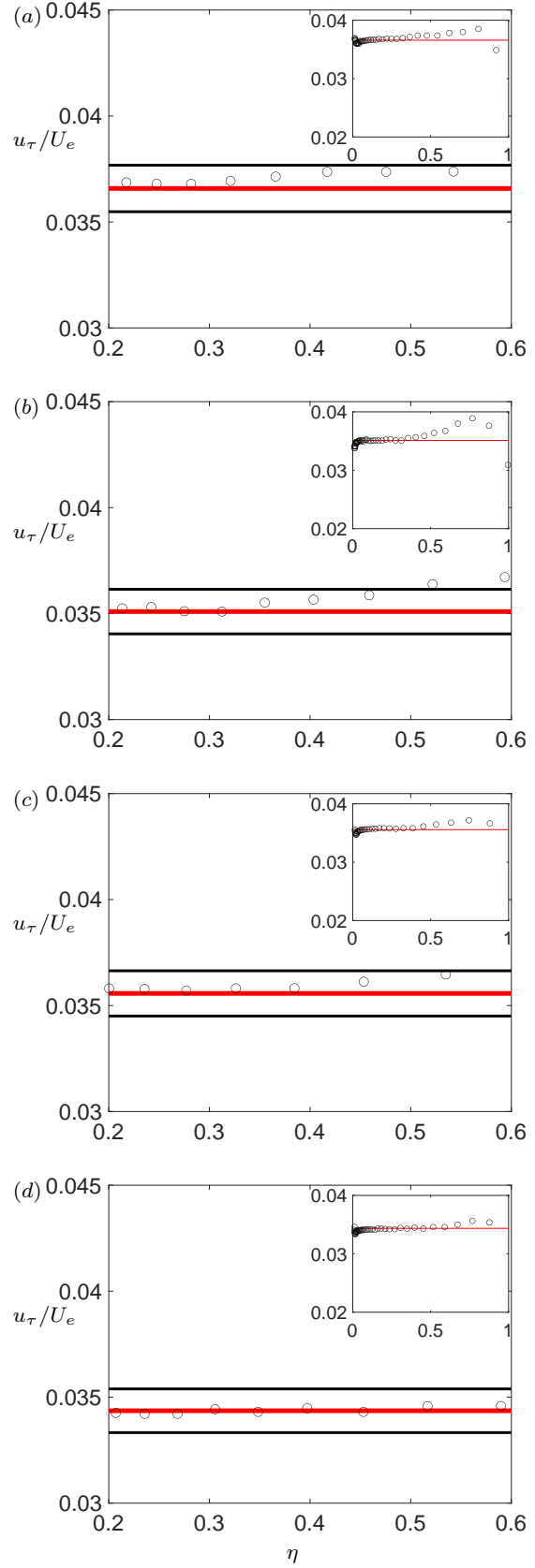


Fig. 6 Predicted u_τ is compared to u_τ obtained from the composite fit (red line) for cases E6920 (a), E9830 (b), E11200 (c), and E15120 (d). Note that the black lines show $\pm 3\%$ of the red line.

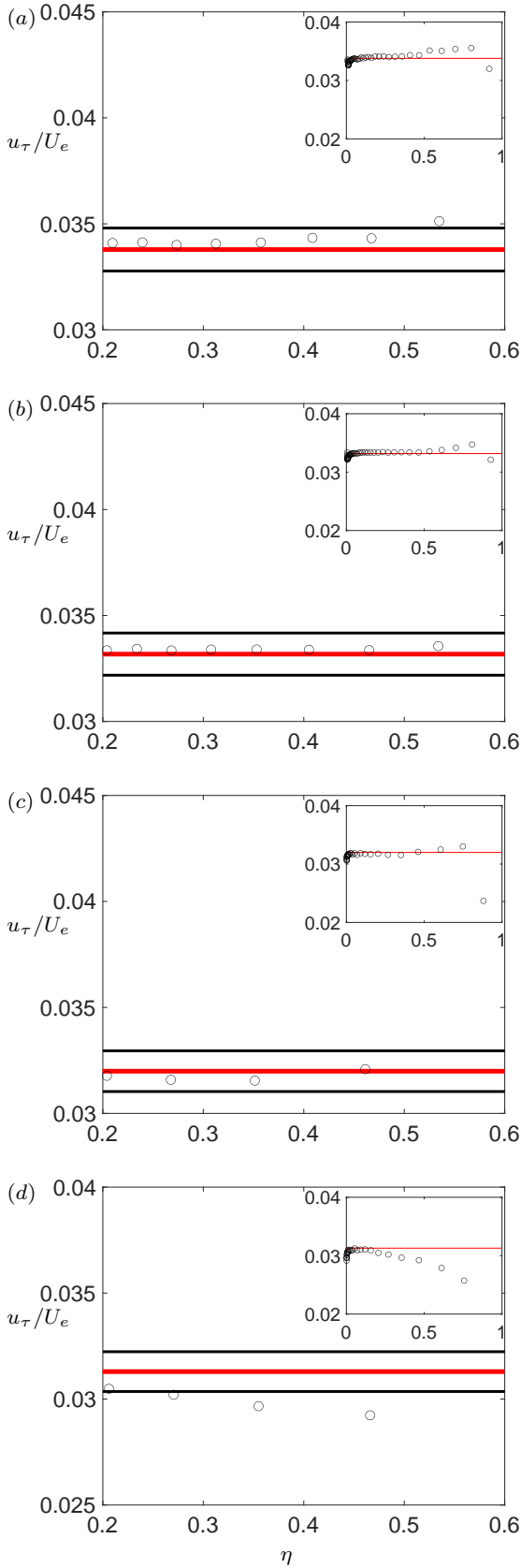


Fig. 7 Predicted u_τ is compared to u_τ obtained from the composite fit (red line) for cases E15470 (a), E24140 (b), E26650 (c), and E36320 (d). Note that the black lines show $\pm 3\%$ of the red line.

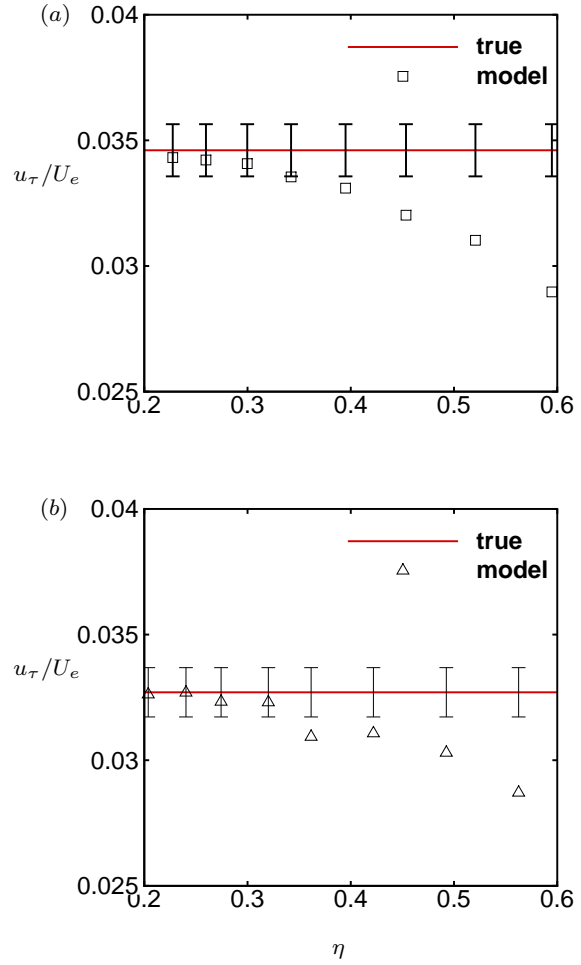


Fig. 8 Predicted u_τ (symbol) is compared to true u_τ (line) for cases E21630 (a) and E51520 (b). Note that the error bar shows $\pm 3\%$ of the red line.

H from the measured data in the absence of near-wall resolution can be challenging. It is tempting to assume the one-seventh power law for near-wall data to account for the contribution of missing data to the overall H . However, the goal here is to avoid using the inner layer altogether. Hence, the sensitivity of the obtained u_τ to H is assessed using error analysis. It can be shown that the relative error in the friction velocity (ϵ_{u_τ}) is related to the relative error in the shape factor (ϵ_H) as

$$\epsilon_{u_\tau} = \left(\frac{0.5H(f - \eta)}{H(1 - f) + (H - 1)(\eta - 1)} \right) \epsilon_H. \quad (16)$$

Figure 10 shows the term in parenthesis on the rhs of Eq. (16) for S1000 and S4000 cases; note that it is of the order 10^{-1} . The term in parenthesis shows a variation in the range 7–12%, which implies that 10% error in H would yield 0.7–1.2% error in the predicted u_τ . Hence, it can be concluded that the predicted u_τ is relatively

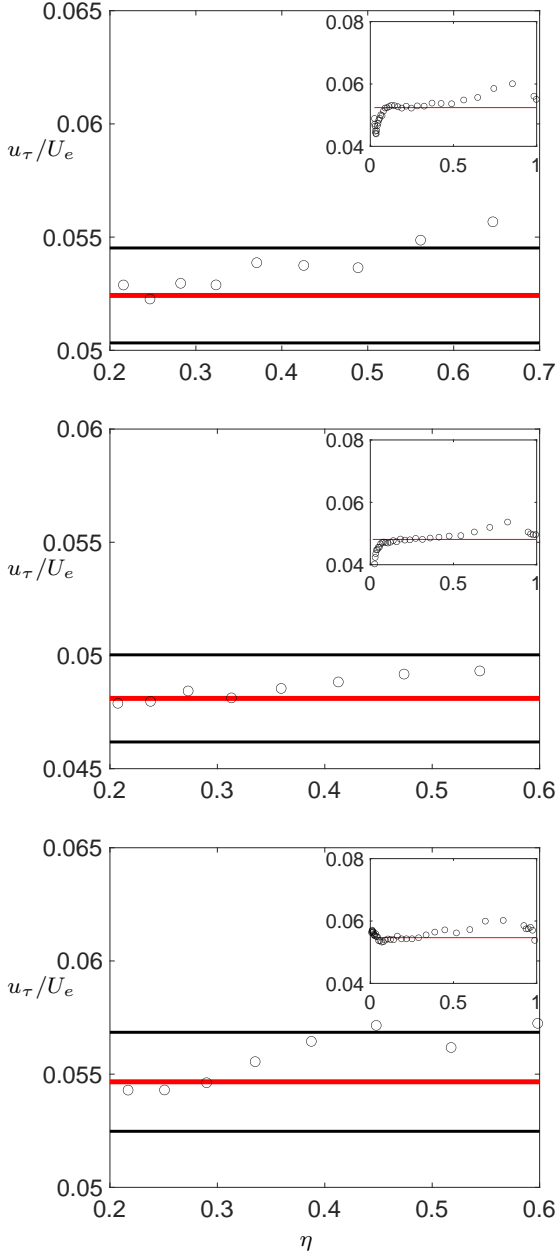


Fig. 9 Predicted u_τ is compared to u_τ obtained from modified Clauser chart method (red line) for cases R0 (a), R- (b), and R+ (c). Note that the black lines show $\pm 4\%$ of the red line.

insensitive to the error in H . Instead of obtaining H from measurements, one can use $H = 1.36$ at high Re (say $Re_\theta > 6500$) without compromising accuracy of the predicted u_τ .

For TBL, δ is not strictly defined. Most studies including the present work assume $\delta \approx \delta_{99}$, i.e. the wall-normal location where $U = 0.99U_e$. However, it has been reported in literature that the δ used in the composite profiles is typically larger than δ_{99} (Samie et al.,

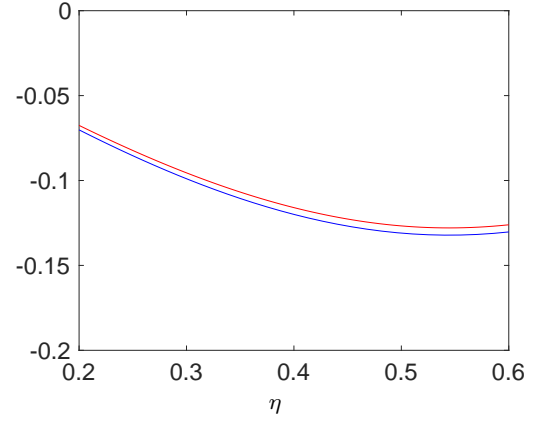


Fig. 10 Sensitivity of the proposed method to the error in H is shown by plotting the term in brackets in Eq. (16) for S1000 (blue) and S4000 (red).

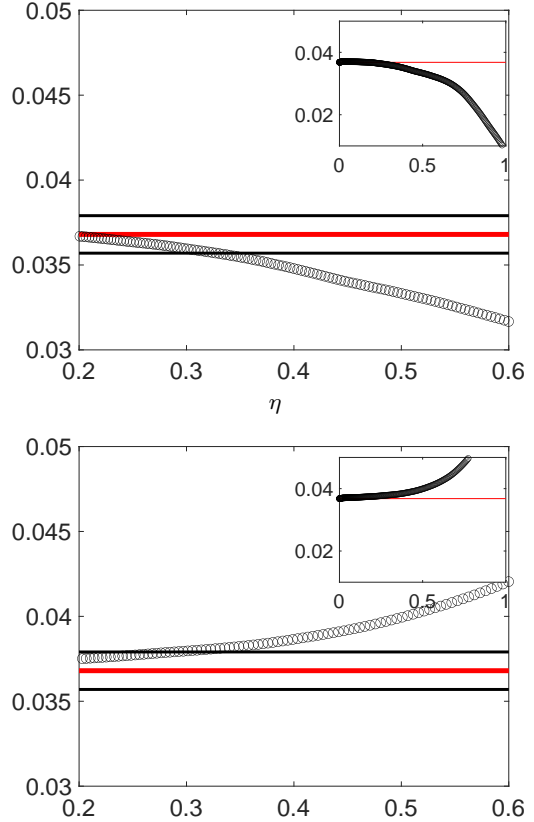


Fig. 11 Sensitivity of the proposed method to the error in δ is shown by using η divided by 1.2 (a) and 0.8 (b) as input to the method and comparing the prediction to true values for S6500 case. Note that the black lines show $\pm 3\%$ of the red line.

2018). Also, iterative integral methods such as that of Perry and Li (1990) yield δ that are up to $\sim 30\%$ larger than δ_{99} . Hence, the sensitivity of the obtained u_τ to δ needs to be assessed. Figure 11 shows the predicted u_τ compared to the reference data for S6500 case if η is divided by a factor of 1.2 (Figure 11a) or 0.8 (Figure 11b), which would correspond to $\pm 20\%$ change in δ . Overall, the method appears robust to errors in δ as long as the data points in the range $\eta < 0.4$ are used. Hence, it can be concluded that the proposed method is robust to the uncertainty in δ and hence $\delta \approx \delta_{99}$ can be used without compromising accuracy of the predicted u_τ .

5 Extension to pressure gradient TBL

A major drawback of the method described in Section 2 is that it can not be used for pressure gradient TBL. In this section, the stress and wall-normal velocity model derivations are revisited to include the effects of pressure gradient on the mean shear stress in TBL.

5.1 Model derivation for T

Using Eqs. 9 and 10, it can be shown that

$$\frac{\partial T}{\partial y} = -U_e \frac{dU_e}{dx} - U \frac{\partial V}{\partial y} + V \frac{\partial U}{\partial y}, \quad (17)$$

where the pressure gradient term in Eq. 10 is replaced by $U_e dU_e/dx$ in Eq. 17. Note that this substitution assumes that $dP/dy = 0$ i.e. $P = P_e$ throughout the boundary layer, which may not be true for general non-equilibrium flows. Integrating Eq. 17 from 0 to a generic y yields,

$$T - \tau_w = -U_e \frac{dU_e}{dx} y + \int_0^y \left(-U \frac{\partial V}{\partial y} + V \frac{\partial U}{\partial y} \right) dy, \quad (18)$$

where τ_w is the mean shear stress at the wall. After normalizing in viscous units, Eq. 18 becomes

$$T^+ = 1 + \eta \beta \frac{\delta}{\delta^*} + I^+, \quad (19)$$

where,

$$I^+ = \int_0^{y^+} \left(-U^+ \frac{\partial V^+}{\partial y^+} + V^+ \frac{\partial U^+}{\partial y^+} \right) dy^+ \quad (20)$$

needs modeling to obtain a model for T^+ via Eq. (19). It is also clear that I is negative and its magnitude should increase away from the wall, since $T^+ > 1$ near wall but 0 at the boundary layer edge.

In order to model I , the first thing to note is that I is a function of y and using Eq. (19), it can be shown

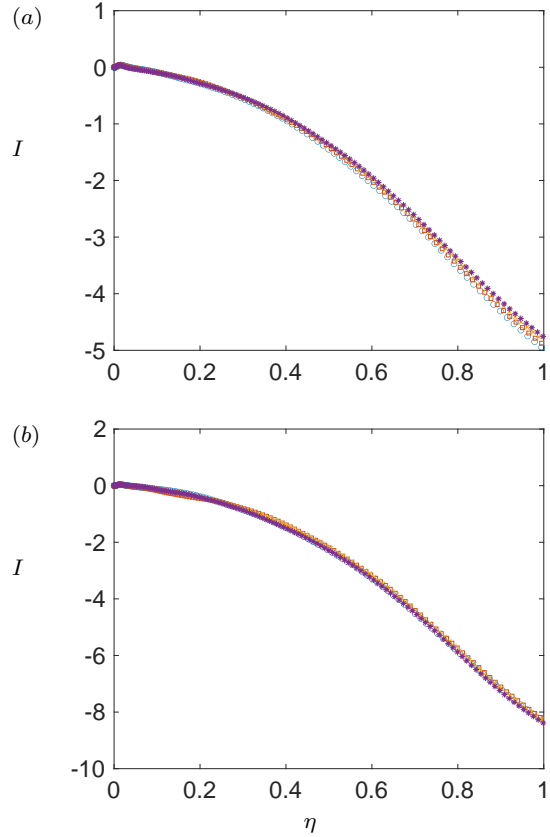


Fig. 12 I profiles for $\beta \approx 1$ (a) and $\beta \approx 2$ (b) are shown.

that I satisfies the boundary conditions

$$I(0) = 0, \quad (21)$$

$$I(\delta) = -\left(1 + \beta \frac{\delta}{\delta^*}\right). \quad (22)$$

The term I is modeled using the existing TBL data from Bobke et al. (2017) as described in Section 3. Figure 12 shows I profiles for $\beta_{11} - \beta_{14}$ and $\beta_{21} - \beta_{24}$ cases listed in table 4. As expected, I is negative and its magnitude monotonically increases away from the wall. The profiles do not collapse. Figure 13 shows the same data after normalizing it with $I(\delta)$. The profiles show excellent collapse to a curve which monotonically increases from 0 to 1 in TBL. The excellent collapse of the data suggests that scaled I is relatively insensitive to Re_τ , which is encouraging for the purpose of model development. Moreover, Eq. (20) suggests that $I^+ \sim U^+ V^+$ implying $I/I(\delta) \sim UV/U_e V_e$. Therefore, a simple modeling choice for I is

$$I = I(\delta) \frac{UV}{U_e V_e}, \quad (23)$$

which combined with Eq. (12) yields a simple model for T^+ as

$$T^+ = 1 + \eta \beta \frac{\delta}{\delta^*} - \left(1 + \beta \frac{\delta}{\delta^*}\right) \frac{UV}{U_e V_e}. \quad (24)$$

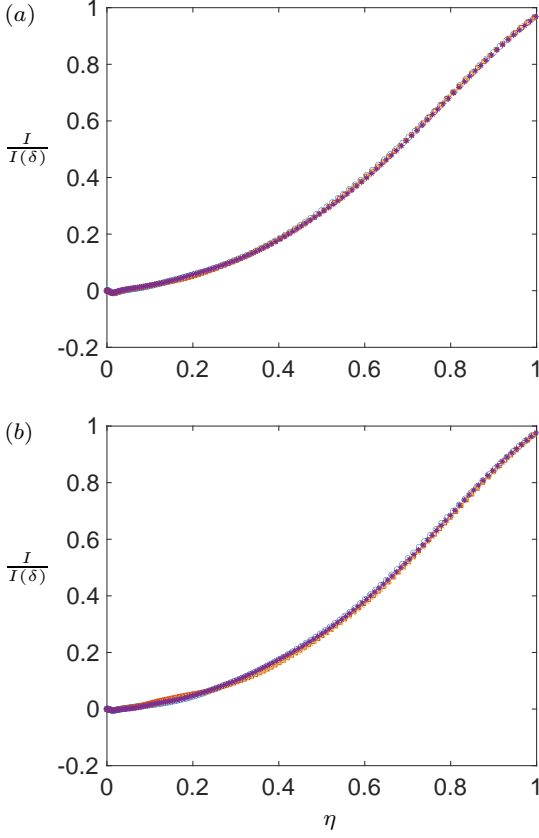


Fig. 13 $I/I(\delta)$ profiles for $\beta \approx 1$ (a) and $\beta \approx 2$ (b) are shown.

It is worth mentioning that the modeling choice of Eq. (23) is not necessarily optimal. It is chosen just for simplicity and it will be shown later that this modeling choice is appropriate for a variety of pressure gradient TBL. The model prediction for T^+ (Eq. (24)) is compared to the reference data in Figure 14 for cases $\beta_{11} - \beta_{14}$ (Figure 14a) and $\beta_{21} - \beta_{24}$ (Figure 14b) respectively. Overall, the model shows good performance despite its simplicity.

Note that Eq. (24) gives a model for T^+ in terms of β , which itself contains u_τ as mentioned earlier. Hence, it is useful to obtain T^+ in terms of K using Eq. (8) to obtain

$$u_\tau = \sqrt{\frac{T + K Re_\delta U_e^2 \left(\eta - \frac{UV}{U_e V_e} \right)}{1 - \frac{UV}{U_e V_e}}} \quad (25)$$

where, Re_δ is the boundary layer thickness based Re . Eq. (25) can be used to obtain u_τ for a pressure gradient TBL if all the terms on the rhs are known. Similar to the ZPG TBL, a model for V is needed if unavailable. The V model of Kumar and Mahesh (2021) (Eq. (14)) was derived for zero pressure gradient TBL and hence, needs extension to include pressure gradient effects.

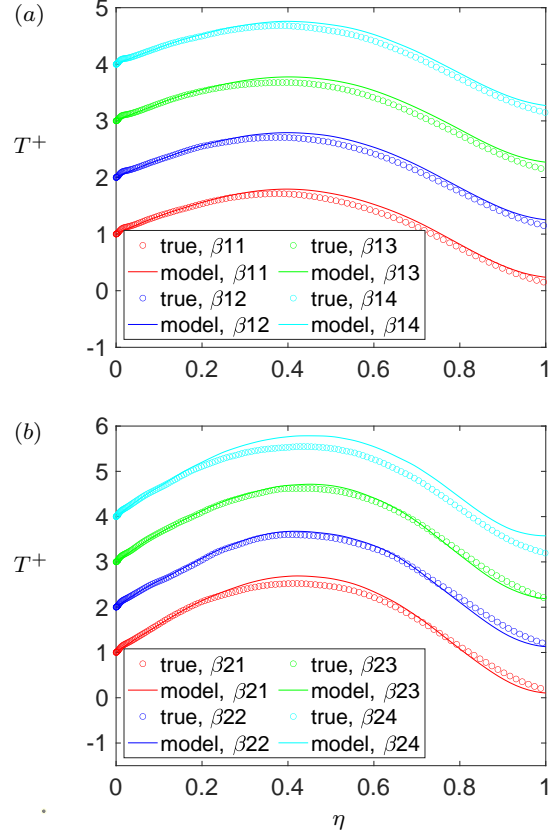


Fig. 14 Modeled T^+ profiles compared to the reference data for $\beta \approx 1$ (a) and $\beta \approx 2$ (b) cases are shown. Note that the profiles are shifted upwards by 1 for clarity.

5.2 Model derivation for V

A key change in TBL behavior under pressure gradient is that V is no longer constant outside TBL. In fact, using the continuity equation (Eq. (9)) it can be shown that

$$\frac{\partial}{\partial \eta} \left(\frac{V}{V_e} \right) = \frac{\beta \delta}{U_e^+ V_e^+ \delta^*} \quad (26)$$

for all $\eta \geq 1$. Also, the edge velocities are related to the boundary layers integral parameters as

$$U_e^+ V_e^+ = H + \beta \left(1 + H + \frac{\delta}{\delta^*} \right), \quad (27)$$

which can be used to obtain V_e (Wei et al., 2017; Kumar and Mahesh, 2018). Figure 15 shows V for four profiles taken each from $\beta \approx 1$ and 2 cases respectively. It is clear that the edge wall-normal velocity obtained using Eq. (27) is able to collapse the profiles to a single curve. Therefore, a model for V/V_e is sought as that can be expected to work for any Re .

The model for V/V_e has two basic requirements: (i) it should reduce to the model of Kumar and Mahesh

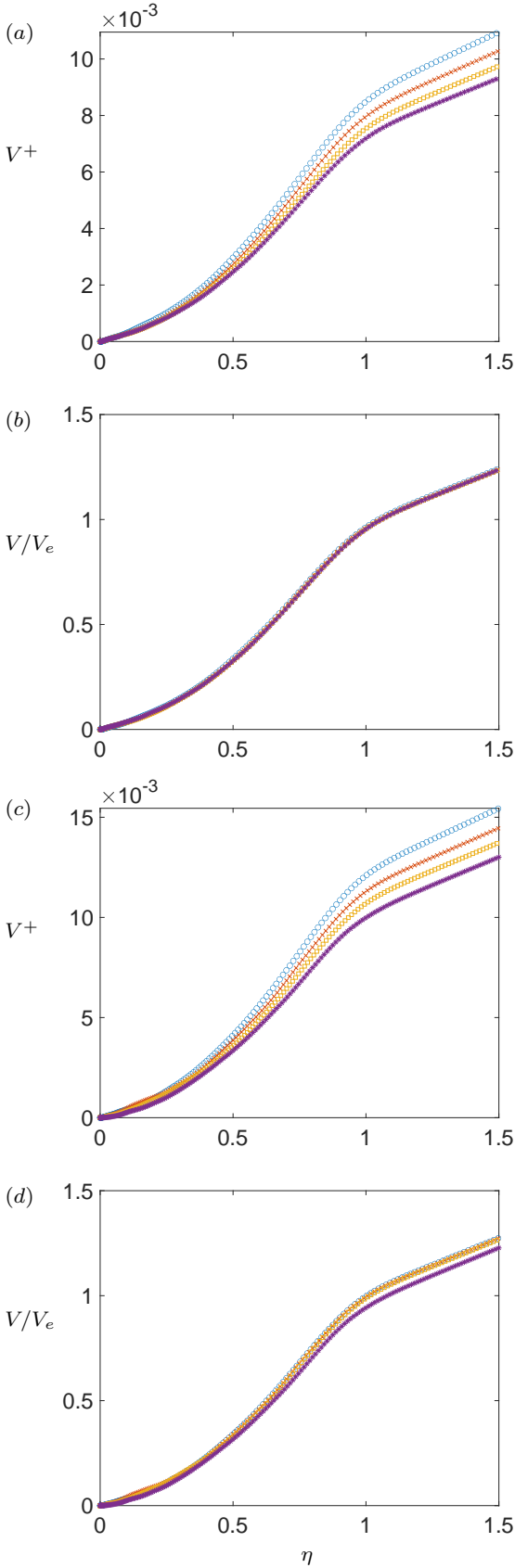


Fig. 15 V^+ (a, c) and V/V_e (b, d) are shown for $\beta \approx 1$ (a, b) and 2 (c, d).

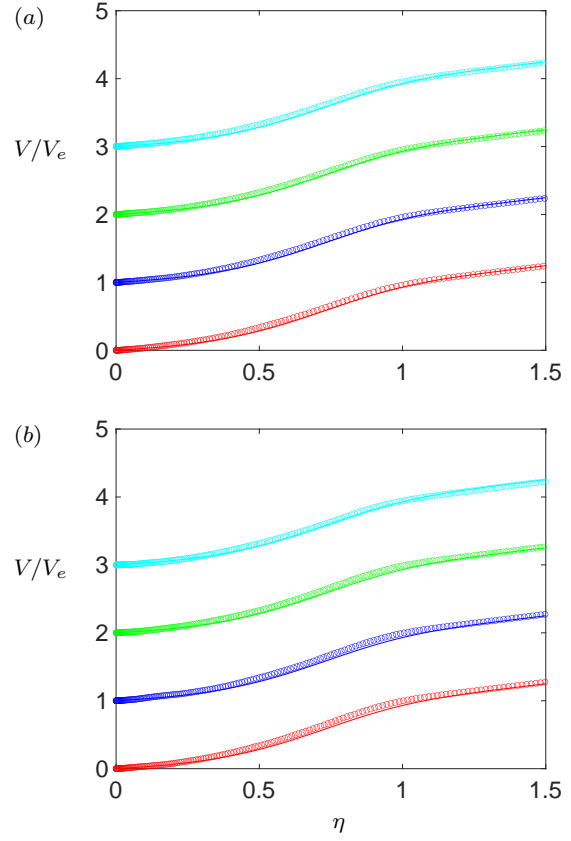


Fig. 16 V/V_e model performance is shown for $\beta \approx 1$ (a) and 2 (b) respectively listed in table 4. Note that the profiles are shifted upwards by 1 for clarity. See Figure 14 for legend.

(2021) for $\beta = 0$, and (ii) it should have the correct slope (Eq. (26)) for $\eta \geq 1$. A convenient choice for such model is

$$\begin{aligned} \frac{V}{V_e} &= \frac{V}{V_e} \Big|_0 \left(1 + \frac{\beta}{U_e^+ V_e^+} \frac{\delta}{\delta^*} (\eta - 1) \right) \\ &= \frac{V}{V_e} \Big|_0 \left(1 - K Re_\delta \frac{U_e}{V_e} (\eta - 1) \right), \end{aligned} \quad (28)$$

where $V/V_e|_0$ is the model of Kumar and Mahesh (2021) (Eq. (14)) and Eq. (8) is used to write β in terms of K .

Next, the performance of the V model is assessed in figure 16 using the same data used in figure 15. The model shows good agreement with the reference data for all the profiles. The model is also tested for constant m cases listed in table 4 as shown in figure 17 showing good agreement for all the cases.

5.3 Discussion

Before proceeding further, it is important to understand key differences in the underlying assumptions of Eq.

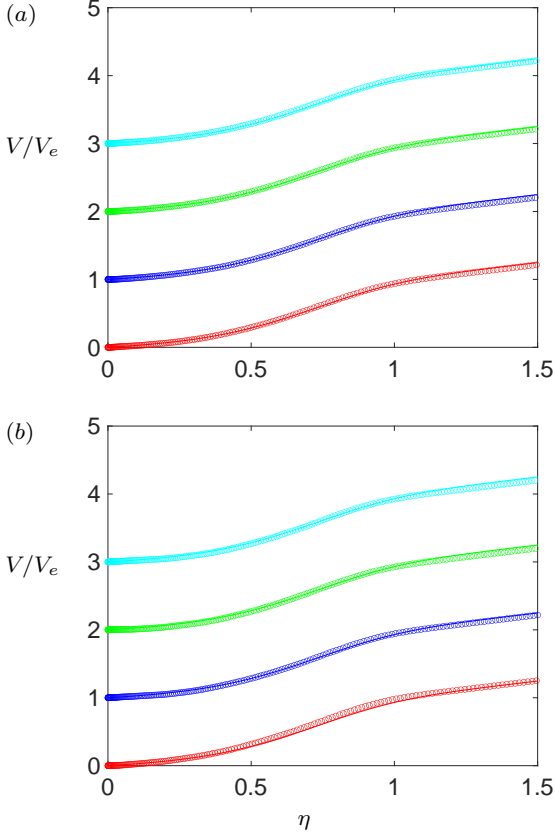


Fig. 17 V/V_e model performance is shown for $m \approx -0.13(a)$ and $-0.16(b)$ respectively listed in table 4. Note that the profiles are shifted upwards by 1 for clarity.

(24) compared to that of Eq. (13). Note that while deriving the latter, both the pressure gradient and the wall-normal velocity terms were ignored and the resulting equation was integrated from a generic y to δ . However, this is not the case for Eq. (19), where both the aforementioned terms are retained and the resulting equation is integrated from 0 to a generic y . This is the reason why setting $\beta = 0$ in Eq. (24) yields a model for T in ZPG TBL as

$$T^+ = 1 - \frac{UV}{U_e V_e}, \quad (29)$$

which is different than Eq. (13). However, both these expressions can be expected to give very similar results for any ZPG TBL. For example, Figure 18 shows comparison between the prediction of Eqs. (13) and (24) for rough wall ZPG TBL data used in figure 9. The smooth wall ZPG TBL cases (not shown here) show similar agreement between the two models.

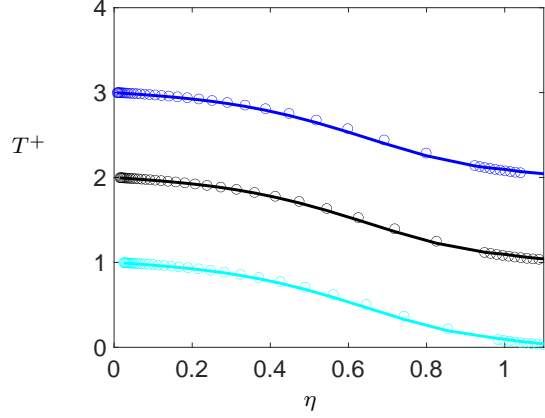


Fig. 18 T^+ profiles predicted by Eq. (24) (symbols) are compared to that obtained from Eq. (13) showing good agreement for R0, R- and R+ cases listed in Table 3. Note that the profiles are shifted upwards by 1 for clarity.

5.4 Method performance for pressure gradient TBL

Two popular methods in literature to determine u_τ from profile data are corrected Clauser chart method and fitting the data to the inner layer profile of Nickels (2004). Both these approaches require accurate near-wall data from the inner layer. For example, Knopp et al. (2021) performed experiments on pressure gradient TBL, where they measured u_τ directly and compared it to that obtained using indirectly using both the aforementioned methods. Their profile measurements had fine resolution near wall as they were able to resolve the buffer layer adequately. They reported an error of approximately 6% using the corrected Clauser chart method and 4% using the latter method. The correction used for the Clauser chart method were empirical. The readers are referred to Knopp et al. (2021) for a detailed discussion on uncertainties of the methods, measurements etc.

Figures 19 and 20 show the predicted u_τ using Eq. (25) for $\beta_{11}-\beta_{14}$ and $\beta_{21}-\beta_{24}$ cases respectively, compared to the reference values. The black lines show the error bounds of ± 8 . Despite simplicity of the model, the prediction is reasonable. It is important to stress again on the fact that the proposed method does not require any near-wall data from the region $\eta < 0.2$. However, if accurate near-wall data are available, the prediction accuracy is improved. For example, if data in the range $0.1 < \eta < 0.2$ were to be used, it appears that the accuracy will be comparable to the existing methods without requiring ad-hoc corrections and parameter tuning.

In order to test robustness, the proposed method is also tested for more challenging constant- m TBL cases

in Figures 21 and 22. The method gives good accuracy for $m131 - m134$. The TBL with $m = -0.16$ is the most challenging pressure gradient case considered in the present work, due to rapid variation of β (Figure 3). However, the overall accuracy is still reasonable for $\eta < 0.35$.

5.5 Sensitivity to TBL parameters

Boundary layer parameters used as inputs to the proposed method for pressure gradient TBL (Eq. (25)) are η , Re_δ and K . It appears that the only source of error can be from the approximation $\delta \approx \delta_{99}$. However, it can be expected that the model performance would not degrade as long as data points are available below $\eta < 0.35$. Note that δ used in the present work is that reported by Bobke et al. (2017), who used the method developed by Vinuesa et al. (2016) to obtain δ from their LES results. H does not appear in Eq. (25), and hence is not required as input to the method.

6 Conclusions

A novel method to determine u_τ from measured profile data is proposed based on the mean stress model of Kumar and Mahesh (2021). The method is based on integral analysis of the governing equations of the mean flow and like all other such methods, requires shear stress profile to determine u_τ . However, unlike all the other methods, the proposed method does not require any near-wall ($\eta < 0.2$) data, thereby avoiding the problems associated with presumption of a universal mean profile and the associated parameters. Unlike most existing methods, the proposed method can handle wall roughness without any modification, and is shown to predict u_τ accurately for a range of Re for both smooth and rough wall TBL. The method requires H and δ as inputs, and it is shown to be relatively insensitive to the uncertainty in these parameters.

Since, the method is based on the mean stress model of Kumar and Mahesh (2021) which was derived for ZPG TBL, it requires extension to include pressure gradient effects. Hence, the model derivation of Kumar and Mahesh (2021) is revisited to obtain novel model for mean stress and wall-normal velocity in TBL including the pressure gradient effects, which is subsequently used to propose a method to reliably determine u_τ from profile data. Therefore, the proposed method provides an alternative to current popular methods to indirectly determine u_τ in TBL within an acceptable uncertainty, and is general enough to handle wall roughness and pressure gradient effects.

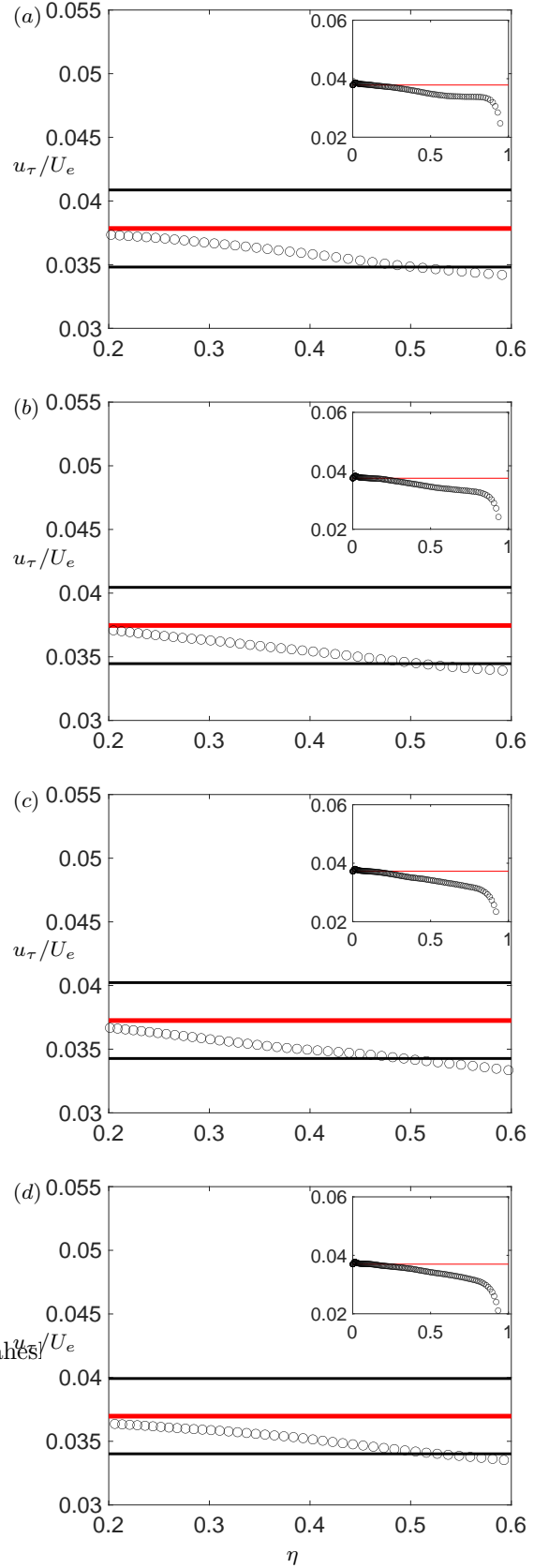


Fig. 19 Predicted u_τ (symbol) is compared to true u_τ (line) for cases $\beta11$ (a), $\beta12$ (b), $\beta13$ (c), $\beta14$ (d). Note that the black lines show $\pm 8\%$ of the red line.

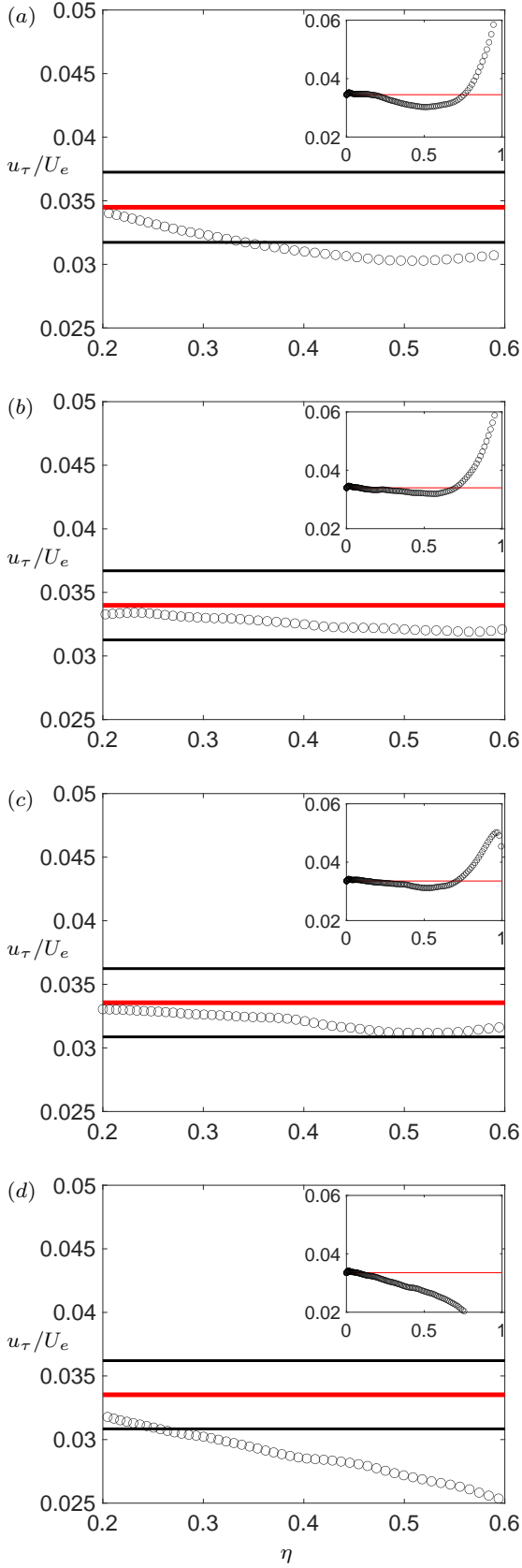


Fig. 20 Predicted u_τ (symbol) is compared to true u_τ (line) for cases β_{21} (a), β_{22} (b), β_{23} (c), β_{24} (d). Note that the black lines show $\pm 8\%$ of the red line.

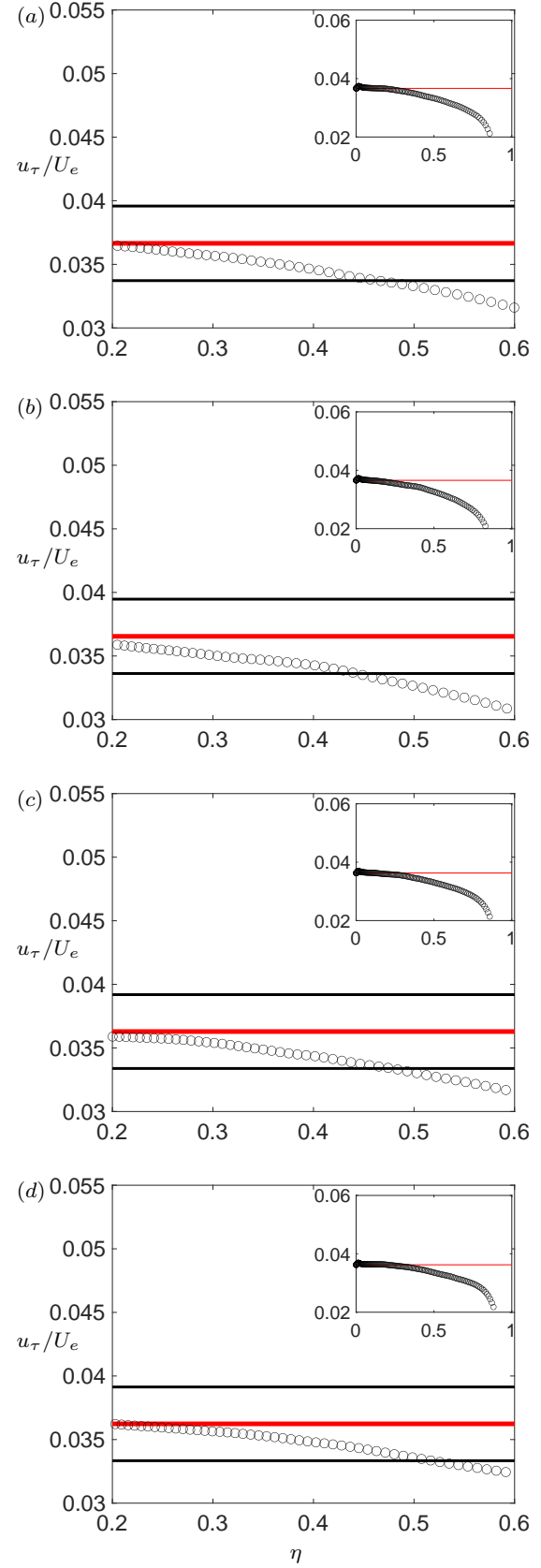


Fig. 21 Predicted u_τ (symbol) is compared to true u_τ (line) for cases m_{131} (a), m_{132} (b), m_{133} (c), m_{134} (d). Note that the black lines show $\pm 8\%$ of the red line.

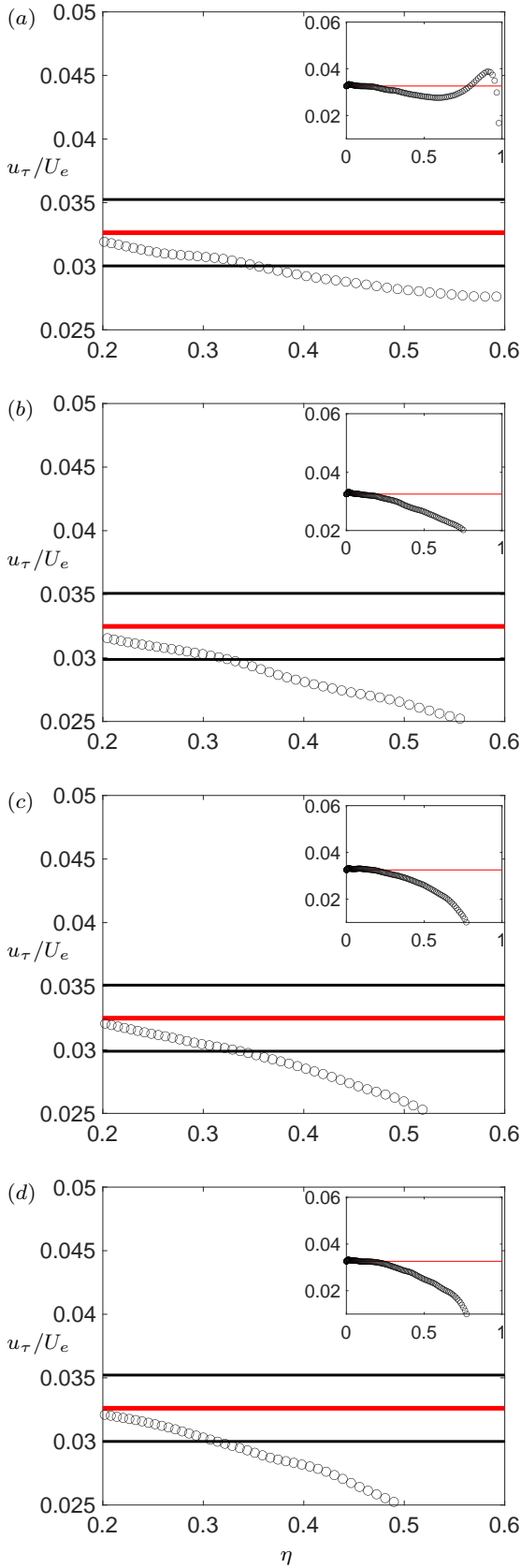


Fig. 22 Predicted u_τ (symbol) is compared to true u_τ (line) for cases *m161* (a), *m162* (b), *m163* (c), *m164* (d). Note that the black lines show $\pm 8\%$ of the red line.

A step-by-step recipe to obtain u_τ from measurement data is as follows:

1. Using measured U profile, obtain δ and hence η , K , Re_δ and V/V_e .
2. Plot the rhs of Eq. (25) in the range $0.2 < \eta < 0.5$ for ZPG or $0.2 < \eta < 0.4$ for pressure gradient TBL.
3. Draw a horizontal line which best-fits the plotted data. Predicted u_τ is the value where this line intersects the y -axis.

The proposed method requires the knowledge of K , U_e and δ , which can be challenging to obtain in pressure gradient TBL. Also, an X-wire probe or PIV might be required to measure T . The method is developed for a spatially growing TBL and hence, it does not work for internal flows such as channel and pipe flows. The method incorporates wall roughness and pressure gradient effects, but requires modifications to account for additional complications like transverse curvature, wall injection or suction etc. Lastly, the accuracy of the method relies on the accuracy of the proposed model for I (Eq. (23)), which appears to be acceptable for the TBL cases shown in the present work. A more accurate model for I has the potential to improve the accuracy of the proposed method further.

Acknowledgements This work is supported by the United States Office of Naval Research (ONR) under ONR Grant N00014-20-1-2717 with Dr. Peter Chang as technical monitor. The authors thank Prof. J. Klewicky for providing the experimental data published in Morrill-Winter et al. (2015).

Conflict of interest

The authors declare that they have no conflict of interest.

References

- Baidya R, Philip J, Hutchins N, Monty JP, Marusic I (2017) Distance-from-the-wall scaling of turbulent motions in wall-bounded flows. *Physics of Fluids* 29(2):020712
- Bobke A, Vinuesa R, Örlü R, Schlatter P (2017) History effects and near equilibrium in adverse-pressure-gradient turbulent boundary layers. *Journal of Fluid Mechanics* 820:667–692
- Chauhan KA, Monkewitz PA, Nagib HM (2009) Criteria for assessing experiments in zero pressure gradient boundary layers. *Fluid Dynamics Research* 41(2):021404

- Clauser FH (1954) Turbulent boundary layers in adverse pressure gradients. *Journal of the Aeronautical Sciences* 21(2):91–108
- Coles D (1956) The law of the wake in the turbulent boundary layer. *Journal of Fluid Mechanics* 1(2):191–226
- De Graaff DB, Eaton JK (2000) Reynolds-number scaling of the flat-plate turbulent boundary layer. *Journal of Fluid Mechanics* 422:319–346
- Fernholz HH, Finley PJ (1996) The incompressible zero-pressure-gradient turbulent boundary layer: an assessment of the data. *Progress in Aerospace Sciences* 32(4):245–311
- Flack KA, Schultz MP, Volino RJ (2020) The effect of a systematic change in surface roughness skewness on turbulence and drag. *International Journal of Heat and Fluid Flow* 85:108669
- Fukagata K, Iwamoto K, Kasagi N (2002) Contribution of reynolds stress distribution to the skin friction in wall-bounded flows. *Physics of Fluids* 14(11):L73–L76
- George WK, Castillo L (1997) Zero-pressure-gradient turbulent boundary layer. *Applied Mech Review* 50(11):689–729
- von Kármán T (1939) The analogy between fluid friction and heat transfer. *Transactions of the American Society of Mechanical Engineers* 61:705–710
- Knopp T, Reuther N, Novara M, Schanz D, Schüle E, Schröder A, Kähler CJ (2021) Experimental analysis of the log law at adverse pressure gradient. *Journal of Fluid Mechanics* 918
- Kumar P, Mahesh K (2018) Analysis of axisymmetric boundary layers. *Journal of Fluid Mechanics* 849:927–941
- Kumar P, Mahesh K (2021) Simple model for mean stress in turbulent boundary layers. *Physical Review Fluids* 6(2):024603
- Marusic I, Monty JP, Hultmark M, Smits AJ (2013) On the logarithmic region in wall turbulence. *Journal of Fluid Mechanics* 716
- Mehdi F, White CM (2011) Integral form of the skin friction coefficient suitable for experimental data. *Experiments in Fluids* 50(1):43–51
- Mehdi F, Johansson TG, White CM, Naughton JW (2014) On determining wall shear stress in spatially developing two-dimensional wall-bounded flows. *Experiments in Fluids* 55(1):1–9
- Monkewitz PA (2017) Revisiting the quest for a universal log-law and the role of pressure gradient in “canonical” wall-bounded turbulent flows. *Physical Review Fluids* 2(9):094602
- Monkewitz PA, Chauhan KA, Nagib HM (2007) Self-consistent high-Reynolds-number asymptotics for zero-pressure-gradient turbulent boundary layers. *Physics of Fluids* 19(11):115101
- Morrill-Winter C, Klewicki J, Baidya R, Marusic I (2015) Temporally optimized spanwise vorticity sensor measurements in turbulent boundary layers. *Experiments in Fluids* 56(12):1–14
- Nagib HM, Chauhan KA, Monkewitz PA (2007) Approach to an asymptotic state for zero pressure gradient turbulent boundary layers. *Philosophical Transactions of the Royal Society A: Mathematical, Physical and Engineering Sciences* 365(1852):755–770
- Nickels TB (2004) Inner scaling for wall-bounded flows subject to large pressure gradients. *Journal of Fluid Mechanics* 521:217–239
- Österlund JM (1999) Experimental studies of zero pressure-gradient turbulent boundary layer flow. PhD thesis, Mekanik
- Perry AE, Li JD (1990) Experimental support for the attached-eddy hypothesis in zero-pressure-gradient turbulent boundary layers. *Journal of Fluid Mechanics* 218:405–438
- Pope SB (2001) *Turbulent flows*. Cambridge University Press
- Prandtl L (1904) Über flüssigkeitsbewegung bei sehr kleiner reibung. *Verhandl III, Internat Math-Kong, Heidelberg, Teubner, Leipzig* pp 484–491
- Prandtl L (1910) Eine beziehung zwischen warmeaustausch und stromungswiderstand der flüssigkeiten. *Phys Z* 11:1072–1078
- Rannie WD (1956) Heat transfer in turbulent shear flow. *Journal of the Aeronautical Sciences* 23(5):485–489
- Reichardt H (1951) Vollständige darstellung der turbulenten geschwindigkeitsverteilung in glatten leitungen. *ZAMM-Journal of Applied Mathematics and Mechanics/Zeitschrift für Angewandte Mathematik und Mechanik* 31(7):208–219
- Rodríguez-López E, Bruce PJK, Buxton ORH (2015) A robust post-processing method to determine skin friction in turbulent boundary layers from the velocity profile. *Experiments in Fluids* 56(4):1–16
- Rotta J (1953) On the theory of the turbulent boundary layer. *NACA Technical Memorandum*, No 1344
- Samie M, Marusic I, Hutchins N, Fu MK, Fan Y, Hultmark M, Smits AJ (2018) Fully resolved measurements of turbulent boundary layer flows up to 20000. *Journal of Fluid Mechanics* 851:391–415
- Schlatter P, Örlü R (2010) Assessment of direct numerical simulation data of turbulent boundary layers. *Journal of Fluid Mechanics* 659:116–126
- Schultz MP, Flack KA (2003) Turbulent boundary layers over surfaces smoothed by sanding. *J Fluids Eng* 125(5):863–870

- Sillero JA, Jiménez J, Moser RD (2013) One-point statistics for turbulent wall-bounded flows at Reynolds numbers up to $\delta^+ \approx 2000$. *Physics of Fluids* (1994-present) 25(10):105102
- Smits AJ, McKeon BJ, Marusic I (2011) High-Reynolds number wall turbulence. *Annual Review of Fluid Mechanics* 43:353–375
- Spalding DB (1961) A single formula for the “law of the wall”. *Journal of Applied Mechanics*
- Taylor GI (1916) Conditions at the surface of a hot body exposed to the wind. *Rep Memo of the British Advisory Committee for Aeronautics* 272:423–429
- Vallikivi M, Hultmark M, Smits AJ (2015) Turbulent boundary layer statistics at very high reynolds number. *Journal of Fluid Mechanics* 779:371
- Vinuesa R, Bobke A, Örlü R, Schlatter P (2016) On determining characteristic length scales in pressure-gradient turbulent boundary layers. *Physics of fluids* 28(5):055101
- Volino RJ, Schultz MP (2018) Determination of wall shear stress from mean velocity and reynolds shear stress profiles. *Physical Review Fluids* 3(3):034606
- Wei T, Klewicki J (2016) Scaling properties of the mean wall-normal velocity in zero-pressure-gradient boundary layers. *Physical Review Fluids* 1(8):082401
- Wei T, Schmidt R, McMurtry P (2005) Comment on the Clauser chart method for determining the friction velocity. *Experiments in Fluids* 38(5):695–699
- Wei T, Maciel Y, Klewicki J (2017) Integral analysis of boundary layer flows with pressure gradient. *Physical Review Fluids* 2(9):092601
- Werner H, Wengle H (1993) Large-eddy simulation of turbulent flow over and around a cube in a plate channel. In: *Turbulent shear flows 8*, Springer, pp 155–168
- Womack KM, Meneveau C, Schultz MP (2019) Comprehensive shear stress analysis of turbulent boundary layer profiles. *Journal of Fluid Mechanics* 879:360–389
- Zhang F, Zhou Z, Yang X, Zhang H (2021) A single formula for the law of the wall and its application to wall-modelled large-eddy simulation. *arXiv preprint arXiv:210409054*